RSC Advances

PAPER

View Article Online
View Journal | View Issue

Cite this: *RSC Adv.*, 2020, **10**, 3438

An L-cystine/L-cysteine impregnated nanofiltration membrane with the superior performance of an anchoring heavy metal in wastewater†

Hong-Li Zhang,‡[a] Huaqiang Cai,‡[b] Yu Xia,[a] Pan Zhang,[a] Si-Wei Xiong[a] and Jing-Gang Gai *[a]

Considerable efforts are being made to develop new materials and technologies for the efficient and fast removal of toxic ions in drinking water. In this work, we developed a sulfur-complexed strategy to enhance the removal capability of heavy metal ions using the polyamide nanofiltration membrane by the covalent anchoring of L-cystine and L-cysteine. The sulfur-functionalized polyamide nanofiltration membrane exhibits superior complexation of heavy metal ions and can efficiently remove them from high-concentration wastewater. As a result, the sulfur-functionalized nanofiltration membrane not only showed excellent desalination performance but also achieved a record removal rate of heavy metal ions (99.99%), which can effectively reduce Hg(II) concentration from 10 ppm to an extremely low level of 0.18 ppb, well below the acceptable limits in drinking water (2 ppb). Moreover, the sulfur-functionalized nanofiltration membrane showed an exciting long-term stability and can be easily regenerated without significant loss of Hg(II) removal efficiency even after six cycles. Such outstanding performances were attributed to the synthetic effect of Hg–S coordinative interaction, electrostatic repulsion, and the sieving action of nanopores. These results highlight the tremendous potential of thiol/disulfide-functionalized NF active layer as an appealing platform for removing heavy metal ions from polluted water with high performance in environmental remediation.

Received 11th November 2019
Accepted 5th January 2020

DOI: 10.1039/c9ra09380j

rsc.li/rsc-advances

1. Introduction

In recent years, water contamination and scarcity have evolved to be a global challenge owing to the rapid growth in population and industrialization.[1–3] One of the major contaminants in drinking and industrial wastewater are heavy metals ions; they are highly toxic and difficult to decompose or metabolize in organisms.[4,5] These heavy-metal ions continuously accumulate to exceed the permissible limits, which vastly threatens public health.[6] In particular, Hg(II) is considered to be the most dangerous heavy metal ion widespread in the environment and it affects the brain, kidney, and lung tissues, severely impairing neurological development and even causing death.[7,8] Therefore, there is a critical need to remove heavy metal ions from polluted water to maintain human and environmental well-being.[9–11]

Among the methods of heavy metal remediation including chemical precipitation,[12] membrane separation, ion exchange,[13] and adsorption,[14–16] membrane separation is the most popularly used due to the advantages of smaller footprint, low-cost, elimination of chemical residuals, relative ease of scaling up, and environmental friendliness.[17–19] As one of the effective means of membrane process, the nanofiltration (NF) technique, which combines the separation mechanisms of size exclusion and Donnan exclusion, has being widely used in drinking water and wastewater treatments because of the higher energy efficiency and simplicity of operation. Currently, the state of the art NF membrane for desalination is composed of a thin film composite (TFC) structure by growing polyamide (PA) nanofilm active layer on a support material,[20] and the permselectivity performance is highly dependent on the molecular and structural characteristics of the PA layer. Since the last few years, researchers have devoted numerous efforts on the modification of TFC nanofiltration separation layer for enhancing the heavy metal removal efficiency. For instance, Chung *et al.*[21] realized higher than 98% rejections of different heavy metals including Pb(II), Cu(II), Ni(II), Cd(II), Zn(II), Cr(VI), and As(V) by employing the chelating polymer modified P84 NF hollow fiber membrane as a separation layer. The poly(amidoamine) dendrimer (PAMAM) was grafted on TFC NF hollow fiber membranes to enhance the heavy metal removal efficiency and achieve an

[a]*State Key Laboratory of Polymer Materials Engineering, Polymer Research Institute of Sichuan University, Chengdu, Sichuan 610065, P. R. China. E-mail: gaijinggang@scu.edu.cn; Fax: +86 28 85402465; Tel: +86 28 85467166*

[b]*Institute of Chemical Materials, China Academy of Engineering Physics, Mianyang 621900, P. R. China*

† Electronic supplementary information (ESI) available. See DOI: 10.1039/c9ra09380j

‡ These authors contributed equally to this work and should be considered co-first authors.

ultrahigh rejection of 99%.[22] In addition, graphene-based materials such as graphene oxide (GO) was also used to improve the heavy metal removal properties of the TFC NF separation layer because of the high porosity, well-defined nanoscale pore size, and suitable mechanical stability.[23,24] Although water permeability is greatly enhanced after the decoration of GO-based frameworks, the undesirable rejection of small ionic species cannot meet the requirement of practical application.[25–27] Currently, the difficulty of constructing the NF membrane mainly lies in enhancing the binding affinity for the target toxic ions to simultaneously achieve the outstanding performance of removal efficiency, selectivity, and reusability. At the same time, the specific and selective elimination of Hg(II) ions from wastewater using separation membranes has scarcely been developed. In this regard, exploring a novel NF membrane material with high efficiency and selectivity for heavy metal removal is mandatory and has been pursued for long.

As a family of soft Lewis bases, sulfur-containing species own a highly polarizable donor center, enabling it to strongly coordinate with low-lying orbitals of soft Lewis acids such as heavy metal ions according to Pearson's theory of Hard/Soft Acids and Bases (HSAB).[28–35] In this context, numerous organic sulfur compounds including thiols, thioethers, disulfides, and mercaptans have been adopted to prepare new materials with high removal efficiency of heavy metal ions such as Hg(II), Ag(I), Pb(II), and Cd(II).[36,37] For example, some thiol/thio-functionalized covalent organic frameworks (COFs), metal–organic frameworks (MOFs), carbon nanotubes, mesoporous silicas, zeolites as well as porous carbons have been developed[38–46] and exhibit high efficiency, selectivity, and easy recyclable adsorption capability towards toxic heavy metal ions. Nevertheless, several drawbacks of these adsorbents are needed to be improved, such as time consumption, production of large amounts of toxic sludge and liquid waste as well as high operational and capital costs.[22] These weaknesses and barriers have sparked our interest in the exploration of new types of materials functionalized with sulfur ligands for water purification. Given all of this, the TFC NF membrane incorporated with sulfur-containing species may be a potential candidate for mitigating environmental problems caused by toxic heavy metals. However, no sulfur-containing species functionalized NF membranes have been reported for effective heavy metal removal from aqueous environments.

Thus, the objective of the present work is to prepare TFC NF active layers functionalized with disulfide (–SS–) and thiol (–SH) groups that are expected to exhibit specific binding ability towards the targeted heavy metals. The surface-bound sulfur ligands enable strong metal-sulfur coordinative interactions, thereby affording efficient and selective removal of toxic heavy metals. Characterizations were conducted to understand the evolution of surface chemistry, morphology, and physico-chemical properties of the membranes before and after modification. Heavy metal ions, including Hg(II), Pb(II), Ni(II), Cu(II), Ag(II), and Cd(II), were also used to test the performance of the pristine and modified membranes. The resultant sulfur-impregnated NF active layers combined exceptional selectivity, good long-term stability, easy regeneration, and unprecedentedly high removal rate of Hg(II) ions (99.99%), making it a highly promising material for decontamination of drinking water. To the best of our knowledge, this is the first attempt towards the use of sulfur-impregnated membrane materials for heavy metal removal studies. This study may open up a new perspective to design advanced TFC NF membrane materials for heavy metal ion removal.

2. Experimental

2.1 Materials

1,3,5-Benzenetricarboxylic chloride (TMC, 98%) and anhydrous piperazine (PIP, 99%) were purchased from Alfa. L-cystine (99%), L-cysteine (99%), $AgNO_3$ (99%), $Pb(NO_3)_2$ (99%), and $NiCl_2 \cdot 6H_2O$ (99%) were obtained from Adamas-beta. $Hg(NO_3)_2$ (99%) was received from Xiya Reagent. *n*-hexane, $Cd(NO_3)_2 \cdot 4H_2O$, $CuCl_2 \cdot 2H_2O$, NaOH, HCl (36.0–38.0%), Na_2SO_4, $MgSO_4$, NaCl, and $CaCl_2$ were bought from Kelong Chemical Reagent Factory (Chengdu, China). All reagents were directly used without further purification. Flat-sheet non-woven-reinforced polysulfone (PSf) ultrafiltration membrane with a molecular weight cut-off of 60 000 as the support was provided by Beijing Haiqingyuan Tech. Co. Ltd and deionized water (3 $\mu S\ cm^{-1}$) was obtained from an ultrapure water treatment system.

2.2 Preparation of the membrane

The sulfur-impregnated NF active layers were prepared *via* a typical two-step interfacial polymerization (IP) reaction (as illustrated in Fig. 1). Specifically, PIP aqueous solution (0.35 wt%) was firstly poured onto the top surface of porous PSf support. After being immersed for 2 min, the excess PIP solution was decanted and the PSf support was air-dried for further reaction. Then, 0.3 wt% TMC hexane solution was rapidly poured on the soaked support for interfacial polymerization. After 1 min, the residual *n*-hexane was removed to terminate the reaction and the freshly prepared PA layer is defined as PIP-TMC. Immediately after this step, an aqueous phase containing L-cystine (1) or L-cysteine (2) was separately poured onto the fresh PIP-TMC surface to react with the residual acyl chloride functional groups. After allowing to react for 2 min, the excess solution was drained off the surface, followed by drying in air for 3 min, then in an oven at 50 °C for 15 min; a sulfur-impregnated PA active layer was obtained. Finally, the fabricated membrane was rinsed with deionized water and stored in $NaHSO_3$ (1 wt%, pH = 12) aqueous solution for performance characterization. The obtained membranes are denoted as 1 or 2-X, where X corresponds to the addition of monomers. Also, 1-0.1 and 2-0.1 are named as NF-SS and NF-SH, respectively. The TFC NF membranes that refer to 3-1 (L-cystine grafted) and 3-2 (L-cysteine grafted) were prepared by the one-step IP technique for comparison with those made by the two-step route. The one-step procedure started with immersion of the PSf support into a mixed aqueous phase containing PIP (0.35 wt%) and L-cystine or L-cysteine (0.1 g) for 2 min and subsequent removal of the excess liquid. Then, the membrane was immersed into a TMC (0.3 wt%) solution in hexane for 1 min and subjected to the same treatment as mentioned above.

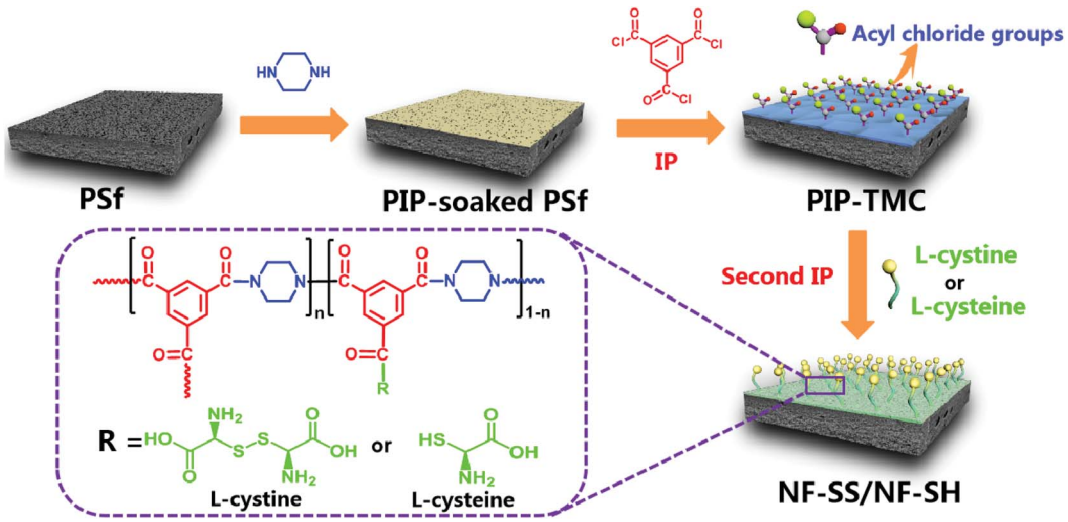

Fig. 1 Schematic representation of the fabrication of sulfur-impregnated NF active layers.

2.3 Membrane characterization

All the membranes were washed with deionized water and dried in a vacuum oven before material characterization. The chemical component of NF selective layers was determined by using a Fourier transform infrared/attenuated total reflectance spectrometer (FT-IR/ATR, Nicolet 380) with an attenuated total reflectance (ATR) unit and an X-ray photoelectron spectrometer (XPS, Kratos, England). The surface and cross-sectional morphologies of the NF layers were investigated by field-emission scanning electron microscopy (FE-SEM, NOVA NANO SEM 450, FEI, USA), atomic force microscopy (AFM, Asylum Research MPD-3d, USA), and transmission electron microscopy (TEM, FEI Tecnai G2 F20, USA). The samples for FE-SEM cross-sectional images were obtained by fracturing the membrane in liquid nitrogen. The surface root-mean-square roughness (RMS) was estimated through the three-dimensional AFM images (5 μm × 5 μm) operated in the tapping mode. To obtain the cross-sections TEM images, the woven fabric substrate (polyester) was carefully removed from the membranes and the NF active layer was embedded with the epoxy resin, then cut at room temperature to obtain the cross-section. Water contact angles (CAs) were measured with a goniometer (DSA30 drop shape analysis system, KRUSS) under sessile drop mode at 25 °C; at least 7 different locations on each sample were tested. Nitrogen-sorption isotherms were obtained from a Quantachrome ASiQwin Instrument. Before the adsorption measurements, the samples were degassed in vacuum at 80 °C for 24 h. The zeta potential of the membrane surface was determined with an electrokinetic analyzer (SurPASS Anton Paar, GmbH, Austria); 1 mM KCl solution served as the background electrolyte and a pH range of 3–10 was adopted.

2.4 Membrane performance test

Water flux and rejection performance of the NF membranes were examined by using a home-made cross-flow filtration instrument with an effective cell area of 60 cm^2, and the operating pressure and temperature were set as 6.0 bar and 25 °C, respectively. 2000 ppm of Na_2SO_4, $MgSO_4$, NaCl, and $CaCl_2$ solutions were used as feed solutions to evaluate the desalination performance. The electrical conductivity of the permeate and feed solutions were measured with a DDS-307 conductivity meter (Shanghai INESA & Scientific Instrument Co. Ltd, China); a calibration curve was used to relate the solution conductivity to the salt concentration. 10 ppm ($Hg(NO_3)_2$, $Pb(NO_3)_2$, $NiCl_2 \cdot 6H_2O$, $CuCl_2 \cdot 2H_2O$, $AgNO_3$, and $Cd(NO_3)_2 \cdot 4H_2O$) solutions were filtered through the separation layers to estimate the heavy metal ion removal property, and the concentrations of the feed and the permeate were obtained by using atomic absorption spectrophotometry (AAS, VARIAN, SpectrAA 220FS, SpectrAA 220Z) and inductively coupled plasma-mass spectrometry (ICP-MS, VG PQ ExCell, TJA, USA). Experimental data were collected after 1 h-filtration to ensure steady-state flow conditions. The water flux of the NF membranes (J, L m^{-2} h^{-1}) was calculated with eqn (1) and the rejection or removal rate (R, %) was obtained with eqn (2):

$$J = \frac{V}{A \times \Delta t} \quad (1)$$

$$R = \left(1 - \frac{C_p}{C_f}\right) \times 100\% \quad (2)$$

where V (L) is the volume of the collected permeate, Δt (h) is the time elapsed for collecting a required permeate volume, A (m^2) is the superficial area of the membrane, and C_f and C_p represent the solute concentration of the feed solution and the permeate solution, respectively.

3. Results and discussion

3.1 Membrane surface chemical composition

The fabrication process of the sulfur-impregnated NF active layers is schematically illustrated in Fig. 1. The TFC NF active layer was prepared by creating a polyamide selective layer on the porous PSf support *via* a two-step IP reaction. The surface chemical components of the TFC NF active layer were identified

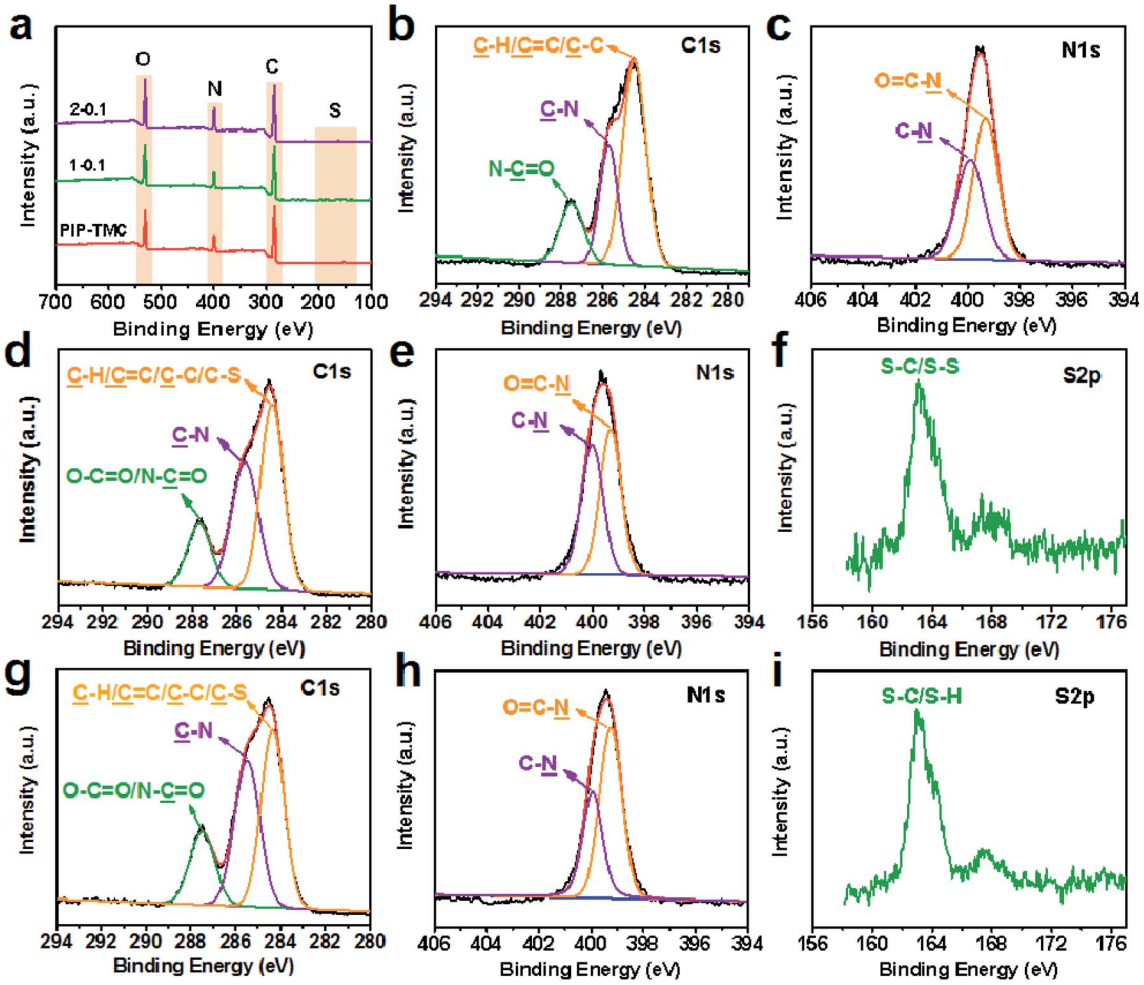

Fig. 2 (a) XPS survey spectra of the NF active layers; high-resolution XPS analysis of (b) C 1s and (c) N 1s of the PIP-TMC active layer; high-resolution XPS analysis of (d) C 1s, (e) N 1s, and (f) S 2p core-level spectra of the NF-SS active layer; high-resolution XPS analysis of (g) C 1s, (h) N 1s, and (i) S 2p core-level spectra of the NF-SH active layer.

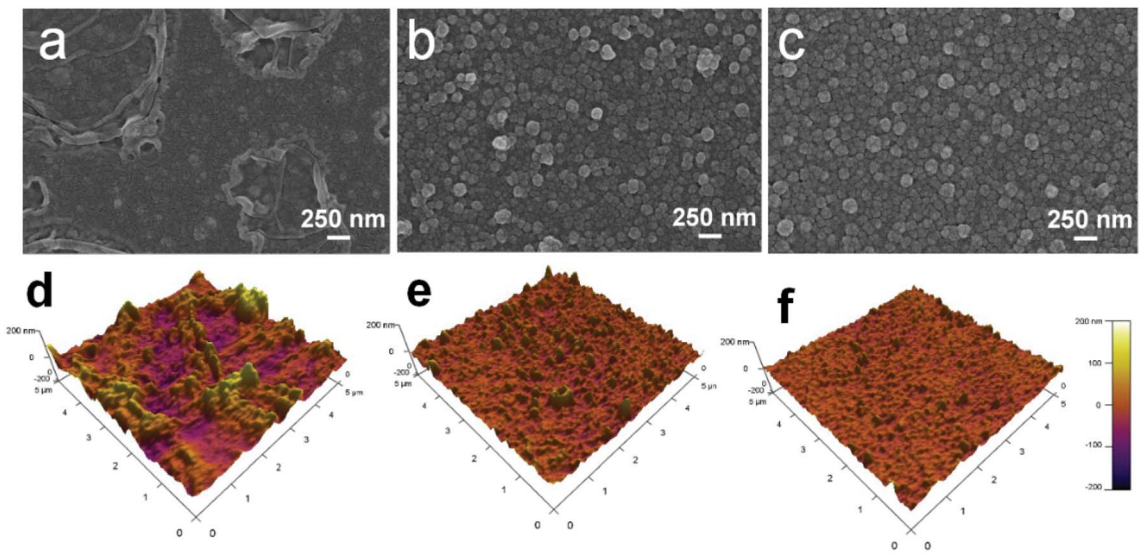

Fig. 3 The surficial-sectional SEM and AFM images of (a and d) PIP-TMC, and (b and e) NF-SS, and (c and f) the NF-SH active layers.

by FT-IR/ATR and XPS techniques. Fig. S1† presents the FT-IR/ATR spectra of the NF membranes. It was found that there appeared a new peak at about 1620 cm^{-1} on the polyamide membrane surface. This peak is ascribed to the stretching vibration of C=O in the amide groups, which reveals that interfacial reaction had successfully occurred and a polyamide active layer was formed on the surface of the PSf support. What should be pointed out here is that we had difficulty in determining the differences between the FT-ATR spectra of PIP-TMC and the sulfur-impregnated active layers. This is probably because the S–H (2500 cm^{-1}), C–S (700–600 cm^{-1}), and S–S (500 cm^{-1}) stretching bands are weak and their peak overlaps with the absorption of other already existing stretching vibrations. The predominant peaks at 285.0 eV, 400.0 eV, and 532.0 eV are facilely assigned to C 1s, N 1s, and O 1s, respectively (Fig. 2a).[47] As evidenced in Fig. 2 and S2,† two eminent peaks of S 2s (231.6 eV) and S 2p (163.0 eV) emerged in the active layers of NF-SS and NF-SH, revealing the existence of the sulfur species.[48] Furthermore, the high-resolution XPS spectra could provide more detailed information on the chemical composition of the NF active layers and thus, the peaks of C 1s, N 1s, and S 2p were deconvoluted into several characteristic peaks under consideration of the elements and the groups directly bonded to the atoms. The C 1s peaks at binding energies of 284.2, 285.4 eV, and 287.6 are assigned to C=C/C–C/C–H, C–N, and N–C=O in PIP-TMC, respectively (Fig. 2b),[49,50] while they are assigned to C=C/C–C/C–H/C–S, C–N, and N–C=O/O–C=O in NF-SS and NF-SH, respectively (Fig. 2d and g). Similarly, the peaks at 399.4 eV and 399.9 eV (Fig. 2c, e, and h) correspond to N–C=O and C–N in the N 1s spectra.[51] The characteristic peaks of S 2p centered at 163.0 eV were detected, as Fig. 2f and i demonstrate, in which the two peaks were respectively assigned to S–C/S–S and S–C/S–H.[52,53] These results signified that the reactant monomers L-cystine and L-cysteine containing –SS– and –SH functional groups have been successfully grafted on the pristine PIP-TMC membrane surface.

3.2 Membrane surface morphology and porosity

The surface morphology of the membranes was characterized by FE-SEM analysis. It could be observed that the nascent active layer shows a nodular surface accompanied by plenty of crumples (Fig. 3a).[51] In comparison, a fairly uniform and obvious grainy surface was generated after the two-step interfacial polymerization, which might be attributed to the smooth surface of the NF-SS and NF-SH active layers. To gain insight into the changes in surface morphology, the surface roughness was examined by employing the AFM technique. A smoother surface could be obviously seen and the RMS values significantly decreased after the impregnation of sulfur species probably because of trampling of L-cystine and L-cysteine chains in the valley structures of the pristine PIP-TMC membrane (Fig. 3d–f), which agree well with the SEM results.[54] At the same time, as Fig. S3† shows, the topography images of the membranes are also highly consistent with the corresponding SEM results. Therefore, the attachment of L-cystine and L-cysteine monomers onto the raw PA layer would not affect the depositions of foulants on the membrane surface caused by surface roughness,[55] which plays a positive role in the antifouling performance of the resultant membrane. Moreover, the cross-sectional SEM and TEM images were also observed. It could be seen that the thickness of the bare NF active layer is about 200 nm, whereas that of the NF-SS and NF-SH layers significantly diminished to 119 nm and 164 nm, respectively (Fig. 4a–c). The reduction in the nanofilm thickness would greatly reduce the resistance to water permeation and thereby facilitate mass transport across the TFC NF barrier layer used for water/wastewater treatment. To gain insight into the porosity properties of the active layers, nitrogen gas sorption

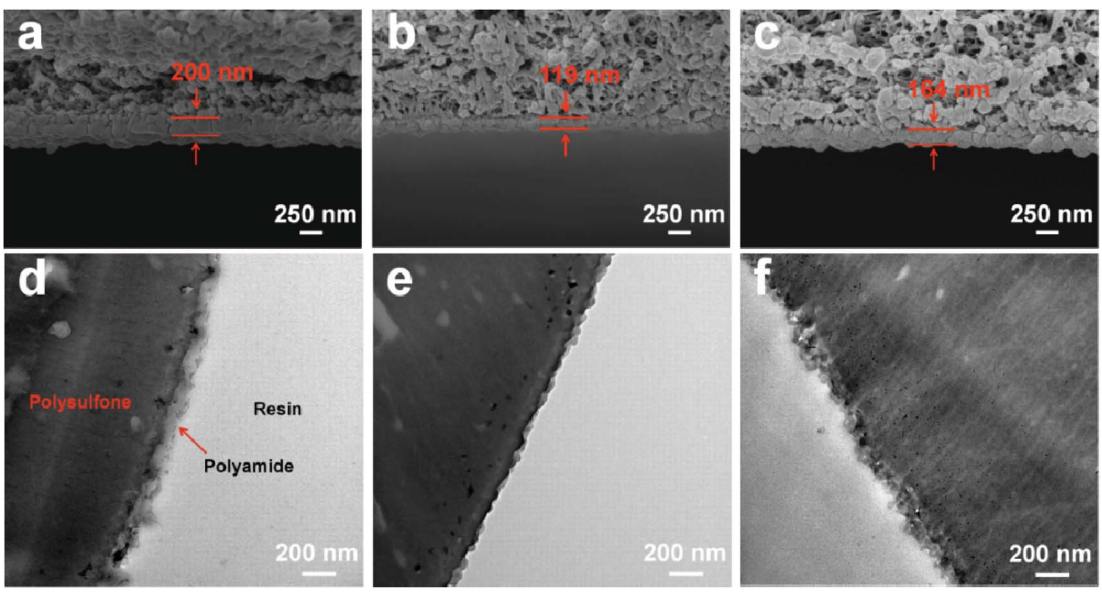

Fig. 4 The cross-sectional SEM and TEM images of (a and d) PIP-TMC, and (b and e) NF-SS, and (c and f) NF-SH active layers.

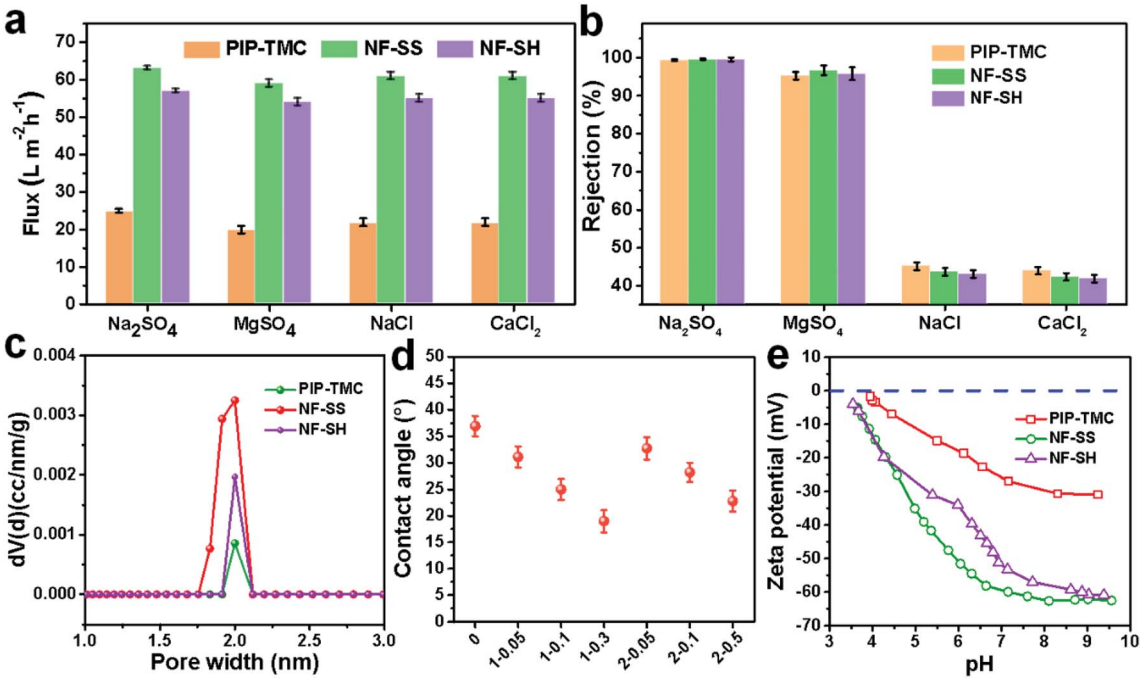

Fig. 5 (a) Water fluxes and (b) rejections of PIP-TMC, NF-SS, and NF-SH active layers for different salt aqueous solution of 2000 ppm at 25 °C and 6 bar; (c) pore size distribution profiles of PIP-TMC, NF-SS, and NF-SH; (d) water contact angles of different NF samples; (e) zeta potentials of PIP-TMC, NF-SS, and NF-SH active layers with increasing pH values.

experiments were carried out. As evidenced by Fig. 5c, the pore size distribution (PSD) curves calculated by using the density functional theory (DFT) method gave a pore size of about 2.0 nm for the PIP-TMC, NF-SS, and NF-SH separation layer, which is characteristic of the NF membrane. The sorption curve at low relative pressures ($P/P_0 < 0.01$) exhibited steep nitrogen uptakes (Fig. S5†), which is indicative of its microporous feature.[56] Such a microporous structure would greatly influence the subsequent separation performance for inorganic salts and heavy metal ions.

3.3 Permselectivity of inorganic salts

In order to evaluate the desalination performance of PIP-TMC, NF-SS, and NF-SH separation layer, the water flux and salt rejection of different membranes were measured with a home-made cross-flow filtration instrument. As Fig. 5a and b show, the desalination performance of NF-SS and NF-SH for all the investigated inorganic salts are significantly improved compared to the traditional PIP-TMC active layer, and achieve a 2.5-fold enhancement in water permeance and an ultrahigh salt rejection. Moreover, the NF-SS and NF-SH active layers display even higher rejections against multivalent anions (99.6%, 99.5% *vs.* 99.3% to Na_2SO_4, 96.7%, 95.5 *vs.*95.3% to $MgSO_4$, 43.7%, 43.1% *vs.* 45.2% to NaCl, 42.4%,41.9% *vs.* 44.0% to $CaCl_2$) (Fig. 5b). These results demonstrate that the grafting of L-cystine and L-cysteine on the PIP-TMC active layer accounts for the enhancement in desalination performance. We reasoned that the high desalting performance of NF-SS and NF-SH is attributed to the more hydrophilic and negative-charged surface. On one hand, the hydrophilic property was examined by comparing the water CAs of the surface before and after impregnation. It could be found that the CA of the NF-SS and NF-SH membranes declined to 25.0° and 28.2°, respectively (Fig. 5d), illustrating that the surface is more hydrophilic surface, thereby favoring the reduction in membrane fouling by hydrophobic foulants.[57] On the other hand, based on the Donnan exclusion theory,[58,59] strong electrostatic repulsion exists between multivalent anions (SO_4^{2-}) and the membrane surface, which decisively influences the multivalent anions passing through the barrier layer of the membranes.[60] It is believed that the surface charge character of the membrane material is closely correlated with the zeta potentials; we therefore measured the zeta potential data in the pH range of 3.0–10.0. Obviously, the NF-SS and NF-SH surfaces tethered L-cystine and L-cysteine monomers bearing an abundance of carboxyl groups have more negative charges than PIP-TMC (Fig. 5e), which thereby enhance the electrostatic repulsive effect between the membrane surface and multivalent anions (SO_4^{2-}), thus endowing the separation with layer higher retention for multivalent anion salts. Taken together, the involvement of L-cystine and L-cysteine resulted in more hydrophilic and negatively charged active layer surfaces, which provide satisfactorily high water permeance while maintaining high selective capability for different inorganic salts.

3.4 Removal performances for heavy metal ions

The flux and removal rate for heavy metal ions of the as-prepared active layers were determined by using 10 ppm heavy metal ion solutions as seed solutions. As Fig. 6a and b illustrate, NF-SS and NF-SH can effectively eliminate toxic ions

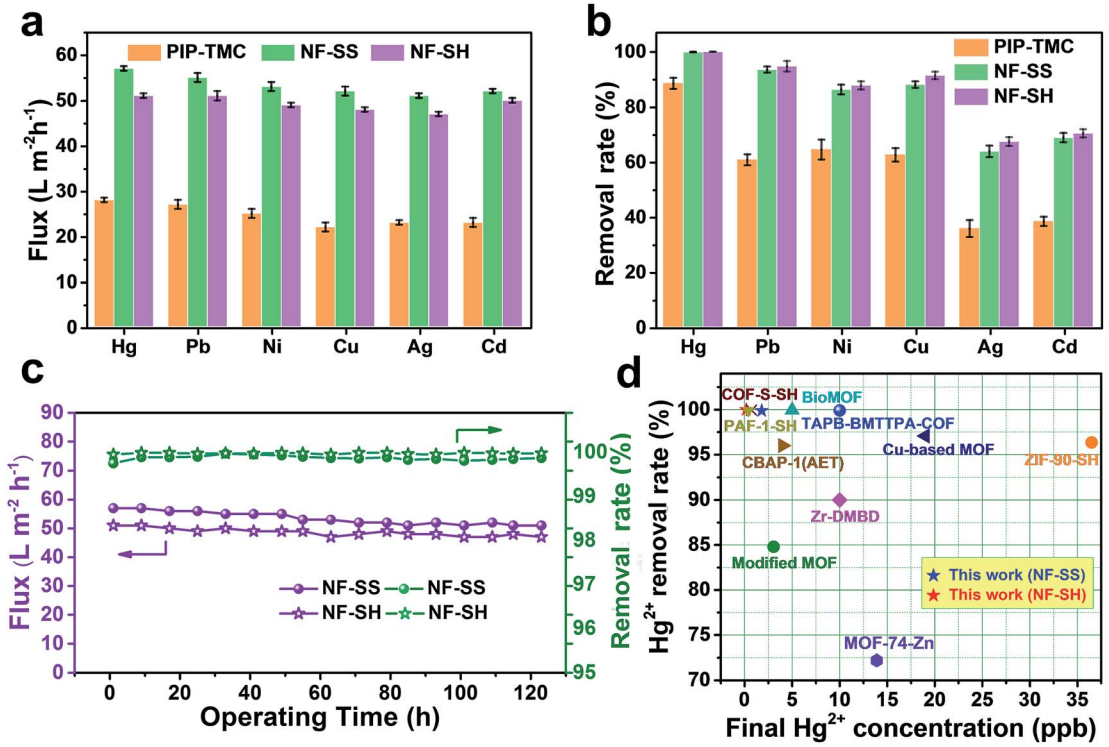

Fig. 6 (a) Water flux and (b) removal rate of PIP-TMC, NF-SS, and NF-SH active layers for different heavy metal ions solutions of 10 ppm at 25 °C and 6 bar; (c) durability of NF-SS and NF-SH in a long-time NF operation process for the removal of Hg(II) ion; (d) comparison of Hg(II) removal performance of recently reported state-of-the-art TFC PA separation membranes and other benchmark thiol/thio-functionalized porous materials (see Table S1† for details).

in water such as Hg(II), Pb(II), Ni(II), Cu(II), Ag(I), and Cd(II) and exhibit excellent water flux. To be specific, NF-SS shows a high removal rate of ~99.98% for Hg(II) and can reduce the concentration of heavily mercury contaminated water down to 1.8 ppb, thus acquiring allowable elemental limits (2 ppb for Hg(II)) in drinking water, which is far beyond that provided by the bare PIP-TMC NF membrane (88.47%). At the same time, NF-SH achieved an unprecedentedly high Hg(II) removal rate of 99.99% and obtained an acceptable mercury level of 0.18 ppb, according to the international standards of U. S. Environmental Protection Agency (EPA) and World Health Organization (WHO).[61] It is also worth mentioning that the sulfur-impregnated NF active layers display the highest removal rate of Hg(II) when compared to other selected heavy metal ions including Pb(II), Ni(II), Cu(II), Ag(I), and Cd(II), thus revealing an outstanding selectivity for different heavy metal ions. Furthermore, we compared Hg(II) ion removal performances of NF-SS and NF-SH with recently reported benchmark porous materials and other state-of-the-art thiol/thio-functionalized materials (ESI, ref. 1–12†).[38–40,45,46] As demonstrated in Fig. 6d, it is can be observed that the Hg(II) removal performance of NF-SH is superior to those of most benchmark materials, such as porous carbon,[46] mesoporous silica (ESI, ref. 6†),[45] and MOF materials (ESI, ref. 1 and 2†).[40] Although COF-S-SH[38] and PAF-1-SH (ESI, ref. 8†) can reduce Hg(II) concentrations to 0.1 and 0.4 ppb, respectively, the ultralong equilibrium time (3–6 h) increases the operational and capital costs, thus precluding any implementation. Comparatively speaking, our newly designed NF active layers used for the purification process within a few minutes can reduce Hg(II) to acceptable concentrations. We surmise that such extraordinary performances are due to the covalent binding of L-cystine and L-cysteine with the –SS– and –SH functional groups in the bare TFC polyamide framework, which demonstrate a great promise for selective and efficient clean-up of heavy metal ions from drinking water.

From the perspective of ecological protection and economic sustainability, long-term cyclic stability of wastewater treatment materials is vital for its realistic application; hence, the demetallization and reuse of NF-SS and NF-SH were investigated. Remarkably, the NF-SS and NF-SH active layers still maintain high removal rate for Hg(II) ions over 120 h of continuous filtration, and no appreciable decline in the permeating flux was observed (Fig. 6c). Further, the Hg(II)-laden NF-SS and NF-SH membranes were easily regenerated by rinsing with an aqueous HCl solution (6.0 M), which resulted in almost 98% and 100% demetallation, respectively; the regenerated NF-SS and NF-SH were then subjected to the next round of Hg(II) decontamination processes. It is notable that NF-SS and NF-SH still retain about 91% and 96% of the original removal rate even after six regeneration and reuse cycles (Fig. 7b),[51] suggesting the sulfur-impregnated NF membrane can work as a promising candidate as a long-term and effective heavy metal-scavenging material. The selectivity of the NF membrane in high concentration and multi-component wastewater is another critical

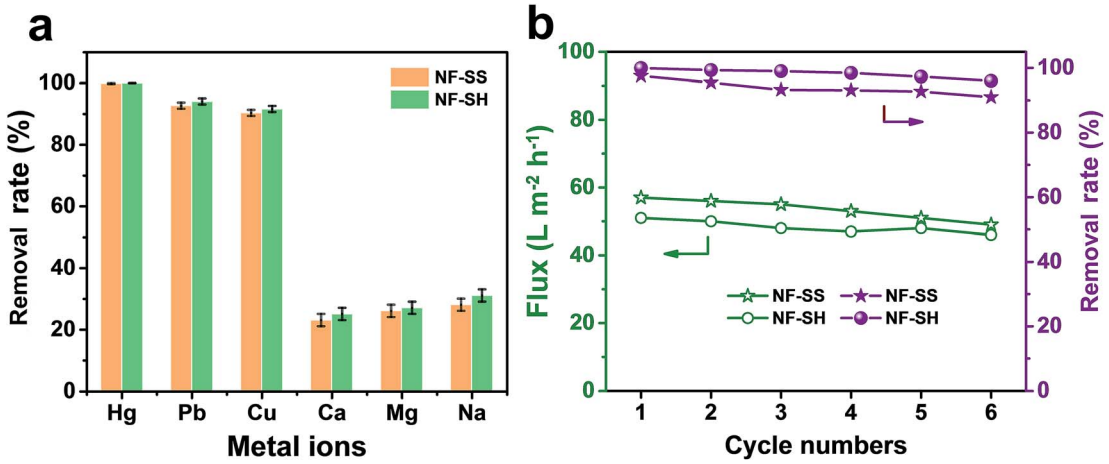

Fig. 7 (a) The removal rate of NF-SS and NF-SH active layers for Hg(II) ion in the presence of other competing metal ions; (b) cycle performance of NF-SS and NF-SH active layers for Hg(II) ion removal.

challenge for practical applications. When the NF membrane is used for water treatment, the different ions will compete for binding sites and the inorganics may block the pores of the NF active layer, thereby compromising the removal efficiency.[40] In light of this, selectivity tests were carried out by using a mixture solution of Hg(II), Pb(II), Cu(II), Ca(II), Mg(II), and Na(I), each at a concentration of 10 ppm, as the seed solution. The results show that NF-SS and NF-SH are capable of removing more than 90% of Hg(II), Pb(II), and Cu(II), and reduce them to drinkable concentrations but they are not active for other metal ions such as Ca(II), Mg(II), and Na(I), thus demonstrating the promising application of sulfur-impregnated NF active layers for the purification of high concentration multicomponent wastewater.

Encouraged by the exceptional performances, we further explored the heavy metal ion removal mechanism of sulfur-impregnated NF active layers, as depicted in Fig. 8. First, –SS– and –SH functional groups are covalently tethered on the surface of the bare polyamide NF membrane. The highly

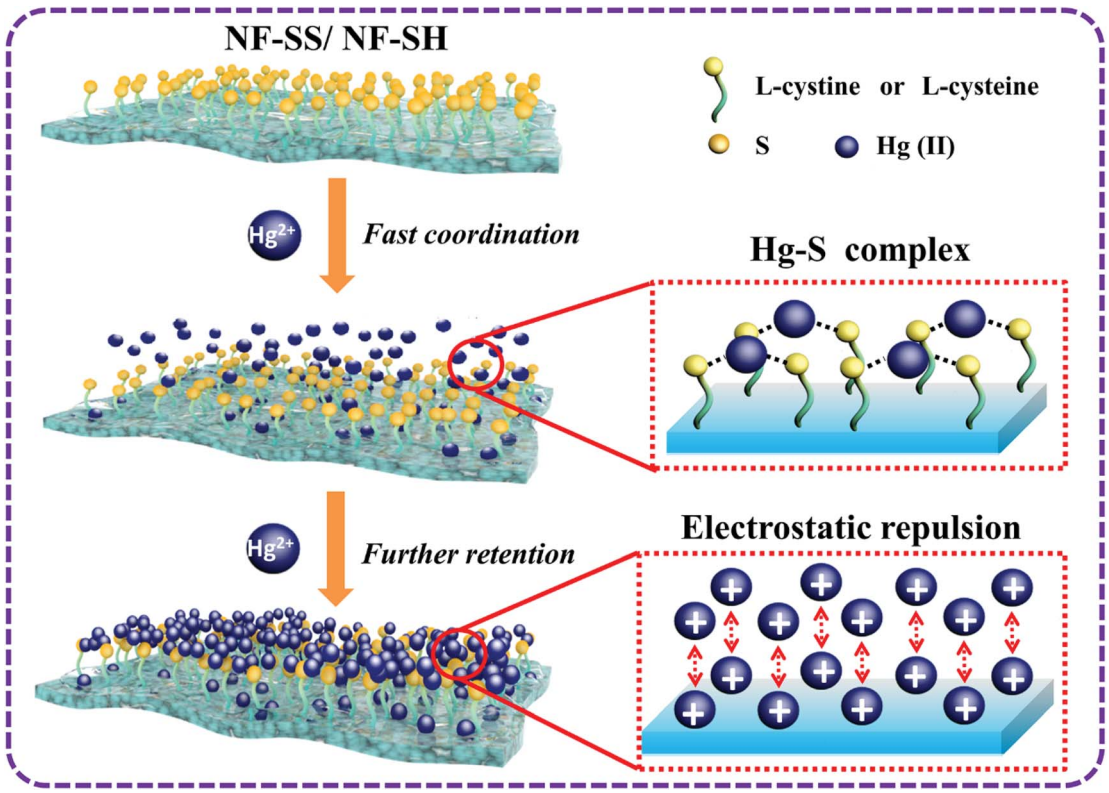

Fig. 8 Suggested mechanism of NF-SS and NF-SH nanofiltration active layers for the removal of Hg(II) ion in multi-metal solution.

accessible and densely populated sulfur species within the polymeric frameworks serve as available soft Lewis bases to bond the soft Lewis acids of heavy metal ions.[28] Second, the hydrated heavy metal ions such as Hg(II) would approach the surface of the membrane quickly, immediately followed by the occurrence of metal-S chelating behavior, which is a spontaneous process propelled by strong and specific surface complexation interactions. As electron acceptors, the empty orbital of heavy metal ions such as Hg(II) could receive electrons from the electron donor of sulfur species to form stable coordination bonds.[35,42] Specifically, each Hg was bound exclusively by two S, that is, Hg(II) ions are complexed in an S–Hg–S bidentate manner, as reported elsewhere.[38,62–65] With respect to the other relatively soft metal ions, such as Pb(II), Cd(II), Ni(II), Cu(II), and Ag(I), due to their lower affinity towards sulfur species than Hg(II), the rejection performances are thereby inferior to that for Hg(II). This is because thiol and disulfide are soft bases groups and hence, they are more likely to attract and interact strongly with soft acids heavy metal ions; among them, Hg(II) is in fact classified as a softer metal than Pb(II) and Cd(II) because of its larger size and greater electron-cloud deformability.[42,63,66–68] As such, the selective separation of Hg(II) from the mixed metal solutions could be well explained. It should also be noted that Hg(II) interaction with –SH groups in NF-SH is more favorable than that with –SS– groups of NF-SS probably due to the steric impediment, thus affording higher removal rate for Hg(II).[62] On the other hand, there exist strong electrostatic repulsions among the multivalent cations (Hg^{2+}) and the positively charged membrane surface contributed by the attachment of Hg(II) ions firstly. Here, the variation in the surface charges of NF-SS and NF-SH were investigated through measurements of the zeta potentials. Obviously, NF-SS and NF-SH surfaces exhibited more positive charge after Hg–S coordination (Fig. S8†), thereby greatly enhancing the electrostatic repulsion and increasing the transfer resistance. It is worth noting that the Hg^{2+} ions in aqueous solution were firmly anchored onto the surface of the membranes and could not drift around, so they would not fill the membrane pores, thereby maintaining high water permeance. Finally, the combination of size exclusion, Hg–S coordinative interactions, and electrostatic repulsion would bring selective and efficient elimination of Hg(II) from polluted water. This heavy metal-scavenging process is fast, highly effective, and the approach is relatively facile, cheap, and highly recyclable, therefore promising the sulfur-impregnated NF membrane with great potential applications in industrial drinking water treatment and environmental remediation.

4. Conclusions

In summary, we have successfully fabricated two sulfur-impregnated composite nanofiltration active layers, NF-SS and NF-SH, that exhibit highly effective and highly efficient removal of selected soft heavy metal ions, especially Hg(II), from heavily contaminated aqueous solutions. Specifically, NF-SH was highly capable of reducing Hg(II) ion concentration from 10 ppm to the extremely low level of less than 0.18 ppb within the drinkable limits of 2 ppb and an unprecedentedly high removal rate of 99.99% for Hg(II) was achieved, outperforming those of the recently reported thiol/thio-functionalized adsorbents and other Hg(II)-scavenging materials. Additionally, the thiol/disulfide-functionalized layers are fully regenerable after six cycles of filtration and demetallization operations, and more than 91% and 96% of the Hg(II) ions can be retained. The sulfur-impregnated TFC membranes can remain effective in the presence of competing metal ions Ca(II), Mg(II), and Na(I), thus illustrating superior selectivity. We surmised that the introduction of sulfur species possessing a high affinity towards soft metals coupled with size exclusion of the NF barrier layer is responsible for the very selective and efficient purification process. When using the sulfur-impregnated NF active layers for desalination, an excellent permeance of 63 L m^{-2} h^{-1} and high rejection greater than 99.6% against Na_2SO_4 can be obtained. Overall, this work provides a facile and time-efficient approach to construct novel NF materials with high desalting capability and outstanding removal performance for heavy metal ions, and demonstrate the prospective application of sulfur-functionalized polyamide NF membrane in the fields of drinking water treatment and environmental remediation.

Conflicts of interest

There are no conflicts to declare.

Acknowledgements

This work was supported by the National Natural Science Foundation of China (51473097), the Sichuan Science and Technology Project (2019YJ0107), and the Opening Project of State Key Laboratory of Polymer Materials Engineering (Sichuan University) (sklpme2014-3-14).

References

1 C. J. Vörösmarty, P. B. McIntyre, M. O. Gessner, D. Dudgeon, A. Prusevich, P. Green, S. Glidden, S. E. Bunn, C. A. Sullivan, C. R. Liermann and P. M. Davies, Global threats to human water security and river biodiversity, *Nature*, 2010, **467**, 555–561.

2 M. M. Mekonnen and A. Y. Hoekstra, Four billion people facing severe water scarcity, *Sci. Adv.*, 2016, **2**, e1500323.

3 I. Haddeland, J. Heinke, H. Biemans, S. Eisner, F. Martina, N. Hanasaki, M. Konzmann, F. Ludwig, Y. Masaki, J. Schewe, T. Stacke, Z. D. Tessler, Y. Wada and D. Wisser, Global water resources affected by human interventions and climate change, *Proc. Natl. Acad. Sci. U. S. A.*, 2014, **111**, 3251–3256.

4 J. Guo, Q. Peng, H. Fu, G. Zou and Q. Zhang, Heavy-metal adsorption behavior of two-dimensional alkalization intercalated mxene by first-principles calculations, *J. Phys. Chem. C*, 2015, **119**, 20923–20930.

5 V. Diana, P. Jemish, Z. Yongfei, Z. Yanli and S. Sánchez, Graphene-based microbots for toxic, heavy metal removal and recovery from water, *Nano Lett.*, 2016, **16**, 2860–2866.

6 X. Li, C. Bian, X. Meng and F. S. Xiao, Design and synthesis of an efficient nanoporous adsorbent for Hg^{2+} and Pb^{2+} ions in water, *J. Mater. Chem. A*, 2016, **4**, 5999–6005.
7 M. Mcnutt, Mercury and health, *Science*, 2013, **341**, 1430.
8 C. J. Clifton, Mercury Exposure and Public health, *Pediatr. Clin. North Am.*, 2007, **54**, 237.e1–237.e45.
9 X. Wang, Z. Z. Zhang, Y. H. Zhao, K. Xia, Y. F. Guo, Z. Qu and R. B. Bai, A Mild and Facile Synthesis of Amino Functionalized $CoFe_2O_4$@SiO_2 for Hg(II) Removal, *Nanomaterials*, 2018, **8**(9), 673–694.
10 Y. H. Zhao, K. Xia, Z. Z Zhang, Z. M. Zhu, Y. F. Guo and Z. Qu, Facile Synthesis of Polypyrrole-Functionalized $CoFe_2O_4$@SiO_2 for Removal for Hg(II), *Nanomaterials*, 2019, **9**, 455–476.
11 K. Xia, Y. F. Guo, Q. J. Shao, Q. Zan and R. B Bai, Removal of Mercury(II) by EDTA-Functionalized Magnetic $CoFe_2O_4$@SiO_2 Nanomaterial with Core–Shell Structure, *Nanomaterials*, 2019, **9**, 1532–1555.
12 M. M. Matlock, B. S. Howerton and D. A. Atwood, Chemical precipitation of heavy metals from acid mine drainage, *Water Res.*, 2002, **36**, 4757–4764.
13 A. Dabrowski, Z. Hubicki, P. Podkoščielny and E. Robens, Selective removal of the heavy metal ions from waters and industrial wastewaters by ion-exchange method, *Chemosphere*, 2004, **56**, 91–106.
14 H. M. Xua, J. P. Jia, Y. F. Guo, Z. Qua, Y. Liao, J. K. Xie, W. F. Shangguan and N. Q. Yan, Design of 3D MnO_2/Carbon sphere composite for the catalytic oxidation and adsorption of elemental mercury, *J. Hazard. Mater.*, 2018, **342**, 69–76.
15 Z. Z. Zhang, K. Xia, Z. W. Pan, C. X. Yang, X. Wang, G. W. Zhang, Y. F. Guo and R. B. Bai, Removal of mercury by magnetic nanomaterial with bifunctional groups and core–shell structure: Synthesis, characterization and optimization of adsorption parameters, *Appl. Surf. Sci.*, 2020, **500**, 143970–143984.
16 C. Zhou, H. Zhu, Q. Wang, J. X. Wang, J. Cheng, Y. F. Guo, X. J. Zhou and R. B. Bai, Adsorption of mercury(II) with an Fe_3O_4 magnetic polypyrrole-graphene oxide nanocomposite, *RSC Adv.*, 2017, **7**, 18466–18479.
17 I. C. Escobar and B. Van der Bruggen, *Modern applications in membrane science and technology*, American Chemical Society Books, Washington, DC, 2011.
18 H. A. Qdais and H. Moussa, Removal of heavy metals from wastewater by membrane processes: a comparative study, *Desalination*, 2014, **164**, 105–110.
19 C. Bellona, J. E. Drewes, P. Xu and G. Amy, Factors affecting the rejection of organic solutes during NF/RO treatment-a literature review, *Water Res.*, 2004, **38**, 2795–2809.
20 Z. W. Jiang, S. Karan and A. G. Livingston, Water transport through ultrathin polyamide nanofims used for reverse osmosis, *Adv. Mater.*, 2018, **30**, 1705973.
21 J. Gao, S. P. Sun, W. P. Zhu and T. S. Chung, Chelating polymer modified p84 nanofiltration (NF) hollow fiber membranes for high efficient heavy metal removal, *Water Res.*, 2014, **63**, 252–261.
22 W. P. Zhu, J. Gao, S. P. Sun, S. Zhang and T. S. Chung, Poly(amidoamine) dendrimer (PAMAM) grafted on thin film composite (TFC) nanofiltration (NF) hollow fiber membranes for heavy metal removal, *J. Membr. Sci.*, 2015, **487**, 117–126.
23 A. K. Geim, Graphene: status and prospects, *Science*, 2009, **324**, 1530–1534.
24 H. Huang, Y. Ying and X. Peng, Graphene oxide nanosheet: an emerging star material for novel separation membranes, *J. Mater. Chem. A*, 2014, **2**, 13772–13782.
25 Y. Zhang, S. Zhang and T. S. Chung, Nanometric graphene oxide framework membranes with enhanced heavy metal removal via nanofiltration, *Environ. Sci. Technol.*, 2015, **49**, 10235–10242.
26 Y. Zhang, S. Zhang, J. Gao and T. S. Chung, Layer-by-layer construction of graphene oxide (GO) framework composite membranes for highly efficient heavy metal removal, *J. Membr. Sci.*, 2016, **515**, 230–237.
27 P. Zhang, J. L. Gong, G. M. Zeng, C. H. Deng, H. C. Yang, H. Y. Liu and S. Y. Huan, Cross-linking to prepare composite graphene oxide-framework membranes with high-flux for dyes and heavy metal ions removal, *Chem. Eng. J.*, 2017, **322**, 657–666.
28 R. G. Pearson, Hard and soft acids and bases, *J. Am. Chem. Soc.*, 1963, **85**, 3533–3539.
29 J. Bao, Y. Fu and Z. Bao, Thiol-functionalized magnetite/graphene oxide hybrid as a reusable adsorbent for Hg^{2+} removal, *Nanoscale Res. Lett.*, 2013, **8**, 1–6.
30 A. Mousavi, Are thiolate anions the only natural organic matter ligands for which mercury(II) has an exceptionally high affinity in aquatic ecosystems?, *Rev. Chim.*, 2015, **66**, 774–777.
31 Y. Li, X. Zhang, B. Zhu, J. Xue and J. Yan, A disulfide-linked naphthalimide dimer for Hg(II) detection in aqueous solution, *J. Fluoresc.*, 2011, **21**, 1343–1348.
32 A. Denizli, K. Kesenci, Y. Arica and E. Pişkin, Dithiocarbamate-incorporated monosize polystyrene microspheres for selective removal of mercury ions, *React. Funct. Polym.*, 2000, **44**, 235–243.
33 S. Bao, K. Li, P. Ning, J. Peng, X. Jin and L. Tang, Highly effective removal of mercury and lead ions from wastewater by mercaptoamine-functionalised silica-coated magnetic nano-adsorbents: behaviours and mechanisms, *Appl. Surf. Sci.*, 2017, **393**, 457–466.
34 C. Zhang, J. Sui, J. Li, Y. Tang and W. Cai, Efficient removal of heavy metal ions by thiol-functionalized superparamagnetic carbon nanotubes, *Chem. Eng. J.*, 2012, **210**, 45–52.
35 F. Rouhani and A. Morsali, Fast and selective heavy metal removal by a novel metal–organic framework designed with in situ ligand building block fabrication bearing free nitrogen, *Chem.–Eur. J.*, 2018, **24**, 5529–5537.
36 K. Chen, Z. Z. Zhang, K. Xia, X. J. Zhou, Y. F. Guo and T. Y. Huang, Facile Synthesis of Thiol-Functionalized Magnetic Activated Carbon and Application for the Removal of Mercury(II) from Aqueous Solution, *ACS Omega*, 2019, **4**, 8568–8579.

37 H. Zhu, Y. Shen, Q. Wang, K. Chen, X. Wang, G. W. Zhang, J. J. Yang, Y. F. Guo and R. B. Bai, Highly promoted removal of Hg(II) with magnetic $CoFe_2O_4$@SiO_2 core-shell nanoparticles modified by thiol groups, *RSC Adv.*, 2017, **7**, 39204–39215.

38 Q. Sun, B. Aguila, J. Perman, L. D. Earl, C. W. Abney, Y. Cheng, H. Wei, N. Nguyen, L. Wojtas and S. Ma, Postsynthetically modified covalent organic frameworks for efficient and effective mercury removal, *J. Am. Chem. Soc.*, 2017, **139**, 2786–2793.

39 N. Huang, L. Zhai, H. Xu and D. Jiang, Stable covalent organic frameworks for exceptional mercury removal from aqueous solutions, *J. Am. Chem. Soc.*, 2017, **139**, 2428.

40 D. T. Sun, L. Peng, W. S. Reeder, S. M. Moosavi, D. Tiana, D. K. Britt, E. Oveisi and W. L. Queen, Rapid, selective heavy metal removal from water by a metal–organic framework/polydopamine composite, *ACS Cent. Sci.*, 2018, **4**, 349–356.

41 M. Mon, X. Qu, J. Ferrando-Soria, I. Pellicer-Carreño, A. Sepúlveda-Escribano, E. V. Ramos-Fernandez, J. C. Jansen, D. Armentano and E. Pardo, Fine-tuning of the confined space in microporous metal–organic frameworks for efficient mercury removal, *J. Mater. Chem. A*, 2017, **5**, 20120–20125.

42 X. Sun, J. Y. Hwang and S. Xie, Density functional study of elemental mercury adsorption on surfactants, *Fuel*, 2011, **90**, 1061–1068.

43 N. M. Bandaru, N. Reta, H. Dalal, A. V. Ellis, J. Shapter and N. H. Voelcker, Enhanced adsorption of mercury ions on thiol derivatized single wall carbon nanotubes, *J. Hazard. Mater.*, 2013, **261**, 534–541.

44 S. Ravi and M. Selvaraj, Incessant formation of chain-like mesoporous silica with a superior binding capacity for mercury, *Dalton Trans.*, 2014, **43**, 5299.

45 O. Hakami, Y. Zhang and C. J. Banks, Thiol-functionalised mesoporous silica-coated magnetite nanoparticles for high efficiency removal and recovery of Hg from water, *Water Res.*, 2012, **46**, 3913–3922.

46 Y. Shin, G. E. Fryxell, W. Um, K. Parker, S. V. Mattigod and R. Skaggs, Sulfur-functionalized mesoporous carbon, *Adv. Funct. Mater.*, 2007, **17**, 2897–2901.

47 S. M. Xue, Z. L. Xu, Y. J. Tang and C. H. Ji, Polypiperazine-amide nanofiltration membrane modified by different functionalized multiwalled carbon nanotubes (MWCNTs), *ACS Appl. Mater. Interfaces*, 2016, **8**, 19135–19144.

48 H. L. Zhang, Y. B. Gao and J. G. Gai, Guanidinium-functionalized nanofiltration membranes integrating anti-fouling and antimicrobial effects, *J. Mater. Chem. A*, 2018, **6**(15), 6442–6454.

49 M. B. M. Y. Ang, Y. L. Ji, S. H. Huang, H. A. Tsai, W. S. Hung, C. C. Hu, K. R. Lee and J. Y. Lai, Incorporation of carboxylic monoamines into thin-film composite polyamide membranes to enhance nanofiltration performance, *J. Membr. Sci.*, 2017, **539**, 52–64.

50 H. L. Zhang, B. H. Liu, M. B. Yang, P. Zhang and J. G. Gai, Sulfaguanidine nanofiltration active layer towards anti-adhesive and antimicrobial attributes for desalination and dye removal, *RSC Adv.*, 2019, **9**(36), 20715–20727.

51 S. H. Huang, C. J. Hsu, D. J. Liaw, C. C. Hu, K. R. Lee and J. Y. Lai, Effect of chemical structures of amines on physicochemical properties of active layers and dehydration of isopropanol through interfacially polymerized thin-film composite membranes, *J. Membr. Sci.*, 2008, **307**, 73–81.

52 H. Zhou, X. Wang, J. Tang and Y. W. Yang, Tuning the growth, crosslinking, and gating effect of disulfide-containing PGMAs on the surfaces of mesoporous silica nanoparticles for redox/pH dual-controlled cargo release, *Polym. Chem.*, 2016, **7**, 2171–2179.

53 S. Park, S. Yang, N. Shin, E. Lee and H. Lee, Adsorption configuration for cysteine on Ge(100): coverage-dependent surface reorientation, *J. Phys. Chem. C*, 2010, **114**, 14528–14531.

54 Y. Gao, S. Zhao, Z. Qiao, Y. Zhou, B. Song, Z. Wang and J. Wang, Reverse osmosis membranes with guanidine and amine enriched surface for biofouling and organic fouling control, *Desalination*, 2018, **430**, 74–85.

55 E. M. Hoek, S. Bhattacharjee and M. Elimelech, Effect of membrane surface roughness on colloid-membrane DLVO interactions, *Langmuir*, 2003, **19**, 4836–4847.

56 R. Dawson, A. I. Cooper and D. J. Adams, Nanoporous organic polymer network, *Prog. Polym. Sci.*, 2012, **37**, 530–563.

57 J. Wang, Z. Wang, J. Wang and S. Wang, Improving the water flux and bio-fouling resistance of reverse osmosis (RO) membrane through surface modification by zwitterionic polymer, *J. Membr. Sci.*, 2015, **493**, 188–199.

58 J. M. M. Peeters, J. P. Boom, M. H. V. Mulder and H. Strathmann, Retention measurements of nanofiltration membranes with electrolyte solutions, *J. Membr. Sci.*, 1998, **145**, 199–209.

59 A. Seidel, J. J. Waypa and M. Elimelech, Role of charge (Donnan) exclusion in removal of arsenic from water by a negatively charged porous nanofiltration membrane, *Environ. Eng. Sci.*, 2004, **18**, 105–113.

60 R. J. Petersen, Composite reverse osmosis and nanofiltration membranes, *J. Membr. Sci.*, 1993, **83**, 81–150.

61 U. S. Environmental Protection Agency, *2012 ed. of the Drinking Water Standards and Health Advisories*, 2012.

62 C. C. Chen, E. J. Mckimmy, T. J. Pinnavaia and K. F. Hayes, XAS study of mercury(II) ions trapped in mercaptan-functionalized mesostructured silicate with a wormhole framework structure, *Environ. Sci. Technol.*, 2004, **38**, 4758–4762.

63 T. Gebremedhin-Haile, M. T. Olguín and M. Solache-ríos, Removal of mercury ions from mixed aqueous metal solutions by natural and modified zeolitic minerals, *Water, Air, Soil Pollut.*, 2003, **148**, 179–200.

64 Y. Oh, C. D. Morris and M. G. Kanatzidis, Polysulfide chalcogels with ion-exchange properties and highly efficient mercury vapor sorption, *J. Am. Chem. Soc.*, 2012, **134**, 14604–14608.

65 Y. Oh, S. Bag, C. D. Malliakas and M. G. Kanatzidis, Selective surfaces: high-surface-area zinc tin sulfide chalcogels, *Chem. Mater.*, 2011, **23**, 2447–2456.

66 M. Khazaei, S. Nasseri, M. R. Ganjali, M. Khoobi, R. Nabizadeh, E. Gholibegloo and S. Nazmara, Selective removal of mercury(II) from water using a 2,2-dithiodisalicylic acid-functionalized graphene oxide nanocomposite: Kinetic, thermodynamic, and reusability studies, *J. Mol. Liq.*, 2018, **265**, 189–198.

67 I. L. Lagadic, M. K. Mitchell and B. D. Payne, Highly effective adsorption of heavy metal ions by a thiol-functionalized magnesium phyllosilicate clay, *Environ. Sci. Technol.*, 2001, **35**, 984–990.

68 A. Denizli, K. Kesenci, Y. Arica and E. Pi şkin, Dithiocarbamate-incorporated monosize polystyrene microspheres for selective removal of mercury ions, *React. Funct. Polym.*, 2000, **44**, 235–243.